JOURNAL OF AIRCRAFT
Vol. 47, No. 2, March–April 2010

Mechanism for Warp-Controlled Twist of a Morphing Wing

Roelof Vos,* Zafer Gürdal,† and Mostafa Abdalla‡
Delft University of Technology, 2629 HS Delft, The Netherlands

DOI: 10.2514/1.39328

A new concept for actively controlling wing twist is described. The concept relied on introducing warping deformation of the wing skin, which was split at the trailing edge to create an open-section airfoil. An internal screw mechanism was introduced near the trailing edge, so that the load-carrying capability of the wing was maintained while allowing the introduction of warping displacement between the lower and upper wing skins at the trailing edge. Simple structural modeling of the warping wing based on generalized thin-walled beam theory was performed. A demonstration wing was built based on a NACA 23012 airfoil section with a span of 0.68 m and a chord length of 0.235 m. A maximum peak-to-peak twist of 27 deg was demonstrated, with excellent correlation between theory and experiment. Wind-tunnel tests showed that warping could change the lift coefficient by as much as 0.7 at maximum peak-to-peak twist. Analytical and vortex-lattice models were demonstrated to give accurate predictions of the lift coefficient at smaller absolute twist angles. Furthermore, analytic modeling of the wing drag was shown to be in close correspondence with the drag measurements and showed that wing warping could be used to influence the lift induced drag. In general, it was demonstrated that at lower angles of attack, a more positive twist resulted in a higher lift-to-drag ratio. This study proved that a twist-active wing can have sufficient gain to control the rolling motion of an aircraft and to ensure that the lift-to-drag ratio is maximized at various flight conditions.

Nomenclature

A	=	area or aspect ratio m^2
b	=	wing span, m
c	=	wing chord, m
c_d, C_D	=	section and wing drag coefficient
c_l, C_L	=	section and wing lift coefficient
E	=	energy, Nm
G	=	shear modulus of elasticity N/m^2
i	=	incidence angle, deg
J	=	torsion constant m^4
L	=	lift, N
s	=	spacial coordinate, m
T	=	torque, Nm
t	=	thickness, m
v	=	induced drag factor due to linear twist
w	=	zero-lift drag factor due to linear twist
α	=	angle of attack, deg
Δw	=	relative trailing-edge warping, m
ϵ	=	washout or washin, deg
θ	=	twist, deg

Subscripts

0	=	zero lift
t	=	tip

Presented as Paper 1879 at the 16th AIAA/ASME/AHS Adaptive Structures Conference, Schaumburg, IL, 7–10 April 2008; received 24 June 2008; accepted for publication 17 November 2009.

*Assistant Professor, Faculty of Aerospace Engineering, Systems Engineering and Aircraft Design, Kluyverweg 1. Member AIAA.

†Aerospace Structures Chair Holder, Faculty of Aerospace Engineering, Kluyverweg 1. Associate Fellow AIAA.

‡Assistant Professor, Faculty of Aerospace Engineering, Aerospace Structures, Kluyverweg 1. Member AIAA.

I. Introduction

CONTROLLED wing twisting can be an effective alternative for ailerons to induce a rolling motion for aircraft [1,2]. In addition, studies showed that controlling the amount of wing twist (washout) during flight can reduce induced drag on all wing geometries, except for the special case of elliptical-wing planforms, resulting in a higher efficiency and a reduced amount of fuel burn [3,4].

In the past, different methods and mechanisms were employed to induce wing twisting. The active flexible wing [5–7] and active aeroelastic wing [8,9] programs investigated the use of leading- and trailing-edge control surfaces to control the wing twist. Although effective, the control system required to achieve these high roll rates was complex and the mechanism could only be employed on relatively thin wings with low torsional stiffnesses. Other aeroelastic methods tailored toward wing twisting involved adaptive attachments, internal stiffness variations, and novel aeroelastic leading-edge and wing-tip devices [10–13]. All aeroelastic approaches use energy from the airstream to induce strain in the structure. Inherent in the concept of aeroelastic flight control is their higher susceptibility to undesired aeroelastic effects (flutter, divergence, and buffet) compared with structures that are designed to suppress these effects.

Inducing twist in a conventional wing structure requires high forces or moments to overcome structural stiffness of the structure [14]. All aeroelastic concepts rely on the airstream to generate these high forces. However, if aeroelastic effects need to stay suppressed, these forces are to be produced by flight control actuators. In that case, most of the energy that is invested in the actuators is dissipated in the straining of the structure, rather than being used to influence the airflow. This imposes stringent requirements on the actuators resulting in an increase in weight, volume, and power consumption compared with conventional actuators that are sized to deflect ailerons.

The torque box structure of a conventional wing is designed to provide a high torsional stiffness to suppress undesired aeroelastic effects such as aileron reversal, divergence, or flutter [15]. A conventional torque box is made of (at least) two spars, the upper and lower skins of the wing, and a series of parallel ribs. The major portion of the torsional stiffness comes from the fact that the cross section of a wing box is a closed section. If a large twisting motion is to be achieved with small torsional loads, then the most effective way of accomplishing this would be to modify the wing box to have an open cross section. In that case, torsion of the wing induces warping of the skin and some of the internal wing box structure. If the rib

sections that close or restrain the torque box are released, the torsional stiffness may be further decreased. However, to be able to achieve active warping of the wing box, reducing the torsional stiffness is not sufficient.

The increased flexibility of a wing box to produce large twisting motion may come at a price of reduced load-carrying capability. To maintain load-carrying capability, positively controlled relative motion of the individual torque box planes needs to be introduced. This can be achieved by either sliding or hinging part of the box structure. By operating this hinging or sliding motion, the amount of warping can be controlled. In turn, the warping induces torsion of the wing structure [16]. The mechanism introduced in this paper addresses one of the key dilemmas of shape-changing structures: *how one can produce large shape changes without losing load-carrying capability*, with the first part requiring reduced stiffness and the latter part needing the stiffness.

The idea behind the present approach is best described by using a simple hollow-tube analogy of a torque box (see Fig. 1). One can imagine the tube to be the external skin of a wing cross section with high torsional stiffness. As mentioned above, by slitting the tube over its entire length, one will be able to twist the tube easily, but the load-carrying capability will be diminished substantially. Depending on the length and cross-sectional area of the tube, the amount of twist could be influenced [16]. It is also important to note that the large twisting motion is also associated with the warping deformation of the tube, with the opposite sides of the slit sliding in the opposite directions. It can easily be demonstrated that a linear differential displacement across the slit could induce torsion. Moreover, if a mechanism used to introduce this differential sliding motion also positively connects the two sides of the slit at all times, then the cross section is no longer open, but closed, keeping the torsional rigidity GJ unchanged. Different actuator arrangements can be used to supply the differential motion along the slit. One of the simple mechanisms to induce the warping deformation is to use a thread rod that goes through small blocks attached to the skins. Before describing the internal wing structure that allows the wing twisting induced by the warping deformation, a simple analysis demonstrating the advantage of a open-section wing skin is presented below to provide an insight into the energy requirement associated with such deformation.

II. Wing Twist Deformation Analysis

Introducing variable torsion in a conventional wing structure means either using powerful actuators or having a flexible wing. The first option requires heavy actuators with large energy requirements, and the latter option can lead to adverse aeroelastic effects. The present wing-warping concept combines both approaches by having a torsionally stiff wing that can be twisted without relying on powerful actuators. To demonstrate that wing twisting according to this approach requires much less energy than for a conventional closed wing section, a qualitative argument is presented in this section.

The reader is asked to consider the wing as being a straight beam (no taper or sweep) that consists of only the wing skin. In that case, the representative cross section has the shape of the airfoil (in this case, a NACA 23012). In Fig. 2 the cross section of this beam has been sketched for two cases: one with a skin that is continuous over the entire perimeter of the airfoil (closed section) and one with a skin that has a discontinuity at the trailing edge (open section). It is

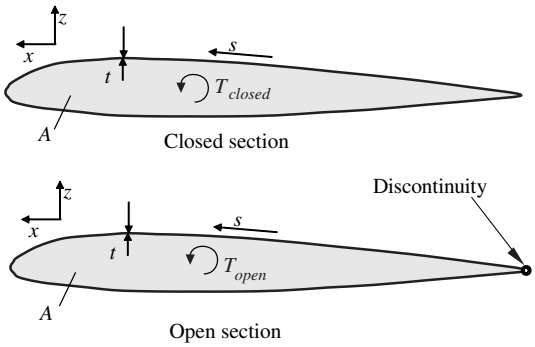

Fig. 2 The wing can be modeled having a closed cross section with a discontinuity.

assumed that the open cross section has the exact same geometry as the closed cross section, except for one discontinuity at the trailing edge. When wing warping is introduced at the trailing edge, the wing can be modeled according to the cross section with discontinuity. If it is assumed that the torsional loads on the wing are transferred solely by shear stresses in the skin, the relative amount of twist in the closed and open sections can be representative of the amount of energy that needs to be provided by the flight control actuators.

The energy E that is required to provide a twist θ in the beam can be expressed as follows:

$$E = T\theta = T\int_0^b \left(\frac{\mathrm{d}\theta}{\mathrm{d}y}\right)\mathrm{d}y \tag{1}$$

where T is the applied torque to the section. For a thin-walled beam section of arbitrary shape, the rate of twist $(\mathrm{d}\theta/\mathrm{d}y)$ is given by the general torsion equation [17,18]:

$$\frac{\mathrm{d}\theta}{\mathrm{d}y} = \frac{T}{GJ} \tag{2}$$

where J is the torsion constant, and G is the shear modulus of elasticity. To induce the same amount of twist in both sections, they are both subjected to different torques (see Fig. 2. In that case, the following identity must hold:

$$\theta = \int_0^b \frac{T_{\text{open}}}{GJ_{\text{open}}}\,\mathrm{d}y = \int_0^b \frac{T_{\text{closed}}}{GJ_{\text{closed}}}\,\mathrm{d}y \tag{3}$$

Assuming that the shear modulus as well as the span is the same for both sections, the ratio of applied torque k between the open and closed sections can be established:

$$k = \frac{T_{\text{closed}}}{T_{\text{open}}} = \frac{J_{\text{open}}}{J_{\text{closed}}} \tag{4}$$

Considering Eq. (1) in conjunction with Eq. (4), it can be seen that k is the factor between the torque required by the closed section and the torque required by the open section to achieve the same amount of wing twist θ.

Following Bredt–Batho theory for a closed thin-walled beam section, the torsion constant J is a function of the enclosed area A and the thickness distribution $t = t(s)$ [18,19]:

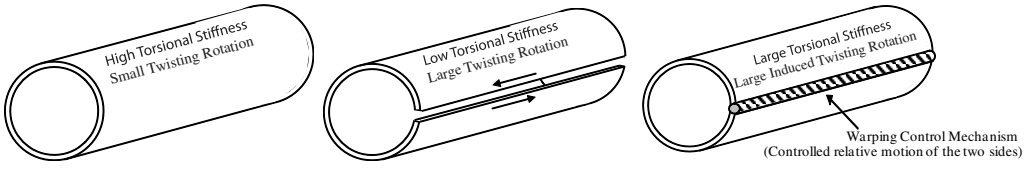

a) Closed tube with high torsional stiffness

b) Open tube with low torsional stiffness

c) Controlled warping with high torsional stiffness

Fig. 1 Basic principle of the warping mechanism.

$$J_{\text{closed}} = \frac{4A^2}{\oint \frac{ds}{t}} \tag{5}$$

For an open thin-walled beam section, the torsion constant is only a function of the thickness distribution [19]:

$$J_{\text{open}} = \frac{1}{3}\int_{\text{sect}} t^3 \, ds \tag{6}$$

Since the open section only differs from the closed section at one discontinuity, the integral

$$\int_{\text{sec t}} t^3 \, ds$$

can be approximated with $\oint t^3 \, ds$. Furthermore, if the perimeter of the cross section is smooth and the thickness t is constant over its entire length, the torque ratio k can be expressed as

$$k = 12\left(\frac{A}{t\oint_s ds}\right)^2 \tag{7}$$

For thin-walled sections, it can be shown that $k \ggg 1$. This proves that for an equivalent amount of twist, a beam with a closed section requires a torque that is k times larger than for a beam with a open cross section, provided that the geometry and stiffness properties are identical for both beams.

For a typical NACA 23012 airfoil with a chord length of $c = 0.235$ m (9.25 in.) and skin thickness of 0.5 mm, the value of k is close to 10^4. Since $E_{\text{open}} = E_{\text{closed}}/k^2$, the energy required to achieve the same amount of twist in the open section is only a fraction of the energy required to twist the closed section. Accordingly, the amount of energy that needs to be invested in the flight control actuators to strain the passive structure can be decreased substantially if a discontinuity is present somewhere in the perimeter of the wing section. The wing-warping mechanism that was presented in Fig. 1 can therefore benefit from relatively lightweight actuators compared with the stout actuators that would be required to twist a similar closed wing section.

III. Design and Manufacturing of a Demonstration Model

A. Overall Design

To demonstrate the effectiveness of wing warping, a demonstration wing was designed and built. The design of this proof-of-concept prototype is based on a NACA 23012 airfoil with a chord length of $c = 0.235$ m (9.25 in.). The internal structure consists of ribs that can rotate about a fixed solid aluminum rod that serves as a main spar. A carbon-fiber-reinforced polymer (CFRP) skin ($t = 0.5$ mm) that is continuous over the perimeter of the airfoil (except for the trailing edge, where upper and lower parts of the skin are separated) is free to slide over the ribs in the axial (along the wing span) direction, but is restrained in the chordwise direction. Similar to the open section of Fig. 2, this construction allows for the warping deformation and the rotation of the skin with respect to the main spar rod, which is necessary to induce twist. Warping is introduced by a thread rod that runs throughout the entire span of the wing near the trailing edge. Figure 3 shows the schematic of the airfoil with the individual structural components. The present internal structure is tailored to the geometry of the airfoil (NACA 23012). This particular airfoil was chosen arbitrarily to prove the concept of wing warping. However, the identical mechanism can be applied to any airfoil shape with sufficient thickness to store the individual structural components. The final demonstration model of the wing is shown in Fig. 4. In the following sections, a description of the internal details of the wing morphing mechanism is provided.

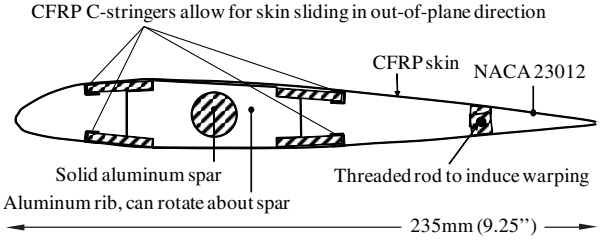

Fig. 3 Side view of structural design of warping wing, including rotating rib and warping mechanism near the trailing edge.

B. Warping Mechanism

Over the span of the wing a thread rod is positioned near the trailing edge to induce the warping deformation between the upper skin and the lower skin (see Fig. 3). The thread rod is connected to the upper and lower skins in such a way that it introduces a relative spanwise movement of the top and bottom surfaces at the trailing edge, referred to as the *warping deformation*. At five trailing-edge stations, equally spaced from each other, the upper and lower skins have three rectangular blocks/houses. The outer two blocks/houses attach to the lower skin and provide guidance of the thread rod. To ensure that the position of the thread rod remains unaltered with respect to the bottom skin, it is kept in place by nuts secured (locked) on the thread rod at the outboard side of each of the sliding houses. The third and middle block attaches to the upper skin and is threaded on the inside. When the thread rod is rotated, the middle block then displaces with respect to the outer two stages. Two of the five stations of the warping mechanism are shown in Fig. 5.

For manufacturing purposes, all of the stations are first attached to two strips of single-layer CFRP: one for the top skin and another for the bottom skin. This ensures the correct spacing of the stations and allows the mechanism to be tested before being integrated into the wing. In a realistic application, the spacing of the individual stations can be optimized such that a more spanwise continuous connection can be made between the upper and lower skins near the trailing edge.

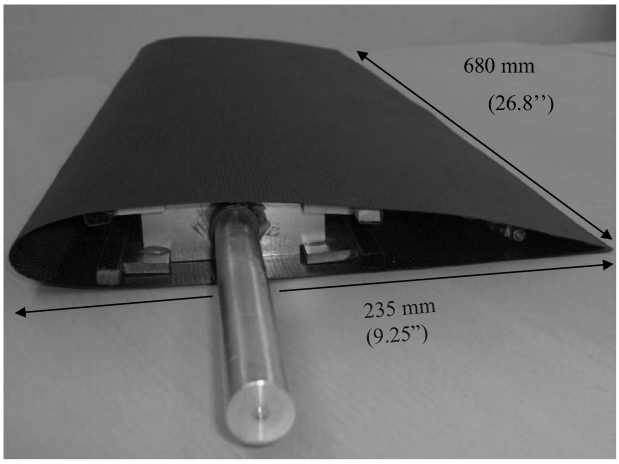

Fig. 4 Finalized wing with CFRP skin and warping mechanism near the trailing edge.

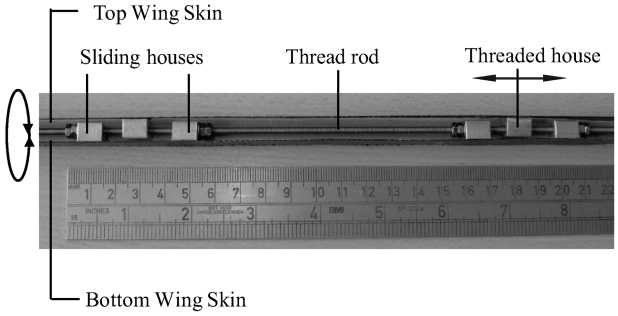

Fig. 5 Two stations of mechanism that induces relative displacement between upper and lower skins.

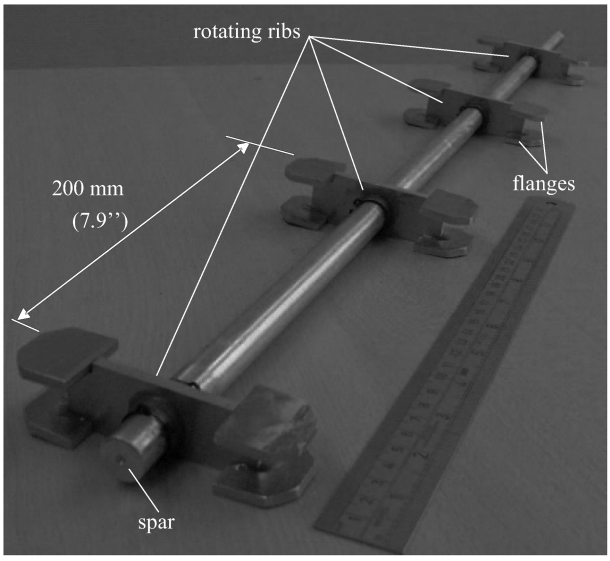

Fig. 6 Internal wing structure consisting of four ribs that rotate independently about the circular main spar.

However, in the present proof-of-concept demonstration model, the position of the stations was chosen for convenient manufacturing reasons.

C. Rib Design and Production

Four ribs, whose shapes are dictated by the outer shape of the airfoil, are equally spaced on the circular spar rod (Fig. 6). To enable rotation about the spar rod, a 20-mm-long hollow tube (inner diameter of 18 mm) is glued inside each of the ribs. This tube ensures perfect rotation without any margins. Position rings at each end of the tubes fixes the location of the ribs on the spar rod. The ribs have four flanges attached to them to help position the skin over them. These flanges are designed to slide into four CFRP guide channels that are glued to the skin. The channels also serve as stiffeners for the skin. Once placed over the ribs with the C-channels going around the flanges, the skin is restrained such that it cannot move in the chordwise direction, but allowed to slide along the spanwise direction, making it possible to induce the warping displacement at the trailing edge. The tips of the flanges of the ribs are rounded to minimize friction during the warping of the wing.

D. Component Integration

The skin is manufactured using a positive/internal mold made out of polyurethane foam. This mold is covered in Mylar (a thin plastic), which prevents adherence of the product to the mold. A single ply of 0–90-weave carbon-fiber cloth is draped over the mold and impregnated with epoxy. No external mold is necessary. The four C-channels attach to the inside of the skin and serve as rails for the rib flanges, such that only a small margin is present between the strips and the flange of the C-stiffeners. This ensures minimal friction during warping deformation of the skin between the C-channels.

IV. Prediction of the Aerodynamic Properties

The focus of this paper is on the introduction of a novel concept for wing morphing. In this section two simple tools are described that can enable a designer to use this technology in future applications.

A. Analytic Model

For attached flow, the lift coefficient C_L of a wing can be expressed as a linear function of the angle of attack α:

$$C_L = C_{L_\alpha}(\alpha - \alpha_{0_L} + i) \tag{8}$$

where i is the incidence angle, α_0 is the angle at which there is no lift generated, and C_{L_α} is the lift-curve slope of the wing. For straight wings subjected to low subsonic velocities, the lift-curve slope is a function of the section lift-curve slope c_{l_α} and the aspect ratio A of the wing [20]:

$$C_{L_\alpha} = \frac{2\pi A}{2 + \sqrt{(2\pi A/c_{l_\alpha})^2 + 4}} \tag{9}$$

The zero-lift angle of attack α_{0_L} is dependent on the section zero-lift angle α_{0_l} and the wing twist at the tip of the wing, ϵ_t. If the airfoil geometry is constant over the span of the wing and a linear twist is assumed, the following relation holds [20]:

$$\alpha_{0_L} = \alpha_{0_l} + \left(\frac{\Delta\alpha_0}{\epsilon_t}\right)\epsilon_t \tag{10}$$

Inserting Eqs. (9) and (10) into Eq. (8) results in the following expression for the wing lift coefficient (assuming there is no incidence angle):

$$C_L = \frac{2\pi A}{2 + \sqrt{(A/c_{l_\alpha})^2 + 4}}\left[\alpha - \alpha_{0_l} - \left(\frac{\Delta\alpha_0}{\epsilon_t}\right)\epsilon_t\right] \tag{11}$$

From a control point of view, it is interesting to know the change in lift coefficient with twist angle. This property can be evaluated by taking the derivative of Eq. (11) with respect to ϵ_t:

$$C_{L_{\epsilon_t}} = \frac{\mathrm{d}C_L}{\mathrm{d}\epsilon_t} = \frac{-2\pi A(\Delta\alpha_0/\epsilon_t)}{2 + \sqrt{(A/c_{l_\alpha})^2 + 4}} \tag{12}$$

The subsonic drag coefficient is found from the addition of the zero-lift drag coefficient C_{D_0} and the lift-induced drag coefficient C_{D_L} [21]:

$$C_D = C_{D_0} + C_{D_L} \tag{13}$$

The lift-induced drag is a quadratic function in ϵ_t:

$$C_{D_L} = \frac{C_L^2}{\pi A e} + 2v\pi C_L\epsilon_t + 4w\pi^2\epsilon_t^2 \tag{14}$$

Table 1 displays the relevant aerodynamic properties of a straight wing (no taper or sweep) with dimensions as shown in Fig. 4 and a NACA 23012 airfoil. Note that this wing is a half-model. By determining its aspect ratio, it was anticipated that for testing, this wing would be clamped to the wind tunnel, which effectively doubled its aspect ratio.

B. Vortex-Lattice Model

To show the validity of the analytical predictions of the morphing wing panel in a flowfield, the MATLAB-based vortex-lattice code Tornado [22] was used. Tornado uses standard vortex-lattice theory, stemming from potential flow theory. In this code, however, the standard horseshoe vortex is replaced by a vortex-sling arrangement.

Table 1 Aerodynamic properties for concept warping wing

Property	Symbol	Value	Units
Section zero-lift angle of attack for NACA 23012 [20]	α_{0_l}	−1.4	deg
Section lift-curve slope for NACA 23012 [20]	c_{l_α}	0.107	1/ deg
Span	b	0.680	m
Chord	c	0.235	m
Aspect ratio	A	5.79	——
Effect of linear twist on wing angle of attack for zero lift [20]	$\Delta\alpha_0/\epsilon_t$	−0.426	——
Oswald span efficiency factor [21]	e	0.90	——
Induced drag factor due to linear twist [21]	v	0.0023	——
Zero-lift drag factor due to linear twist [21]	w	0.0019	——
Zero-lift drag coefficient (measured)	C_{D_0}	0.027	——

This basically works in the same way as the horseshoe, with the exception that the legs of the horseshoe are flexible and consist of seven (instead of three) vortices of equal strength. This enables a more accurate prediction of flapped panels [22].

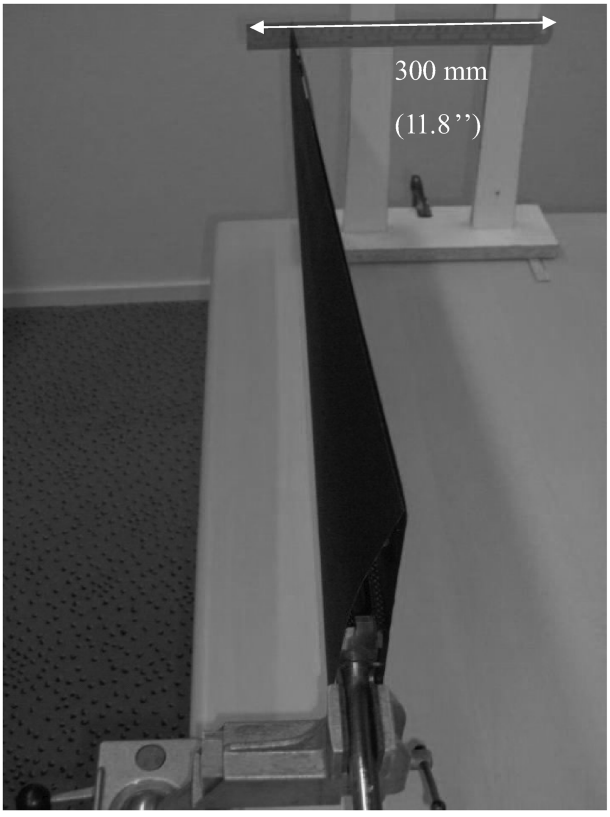

a) Maximum wash-out (negative twist)

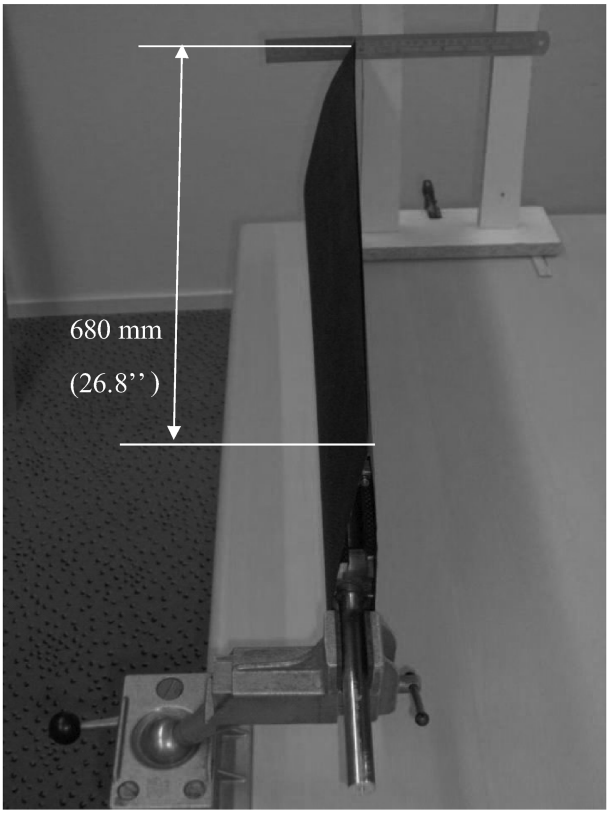

b) Maximum wash-in (positive twist)

Fig. 7 Bench-test setup.

The wing was modeled as being straight, with a NACA 23012 airfoil and with dimensions as displayed in Table 1. Since wind-tunnel tests were to be done on a semispan wing, the wing was mirrored in the xz plane to obtain results that could be compared with the wind-tunnel experiment. Each semispan of the wing was divided into six spanwise panels that were in turn split into four chordwise panels, resulting in a lattice of 24 panels. Linear twist between the root and the tip was assumed and the airfoil section was assumed to be constant over the entire span of the wing. The vortex-lattice model was solely used to calculate the wing lift coefficient rather than a detailed pressure distribution. This way, the predictions could be compared with wind-tunnel balance measurements.

V. Experimental Testing and Results

A. Static Deflection Tests

The twist at the tip of the wing, $\theta = \epsilon_t$, is often referred to as *washout* (if there is negative twist) or *washin* (if there is positive twist) [23]. The airfoil section in Fig. 2 can be modeled as a continuous surface with a discontinuity at the trailing edge, representing the slit that is used for inducing the warping displacement. A linear relationship between the relative trailing-edge warping displacement Δw and the amount of twist at the tip of the wing, ϵ_t, exists [16,19]:

$$\epsilon_t = \int_0^b \frac{\mathrm{d}\theta}{\mathrm{d}y}\,\mathrm{d}y = \frac{b}{2A}\Delta w \tag{15}$$

where $A = 6125\ \mathrm{mm}^2$ is the area that is enclosed by the airfoil perimeter and $b = 680$ mm is the span of the wing panel.

To verify this relationship between twist and warping displacement a bench test was carried out. Warping of the wing was determined by measuring the relative displacement of the upper skin with respect to the lower skin at the trailing edge. This could be easily deduced by multiplying the number of revolutions of the thread rod by its pitch. The horizontal trailing-edge displacement at the tip of the wing was measured using a metric ruler. Assuming small angles of twist, this displacement could be transferred to the angle of twist using simple geometric relations. Figures 7a and 7b show the experimental setup and give an impression of the maximum measured washout and washin.

The results from the bench test are displayed in Fig. 8. The tests showed a linear relationship between the displacement of upper and lower skins, Δw, and the amount of twist ϵ_t and a close correlation with the analytic prediction [Eq. (15)]. Furthermore, the test showed that the maximum peak-to-peak twist that could be attained for this wing was approximately 27 deg.

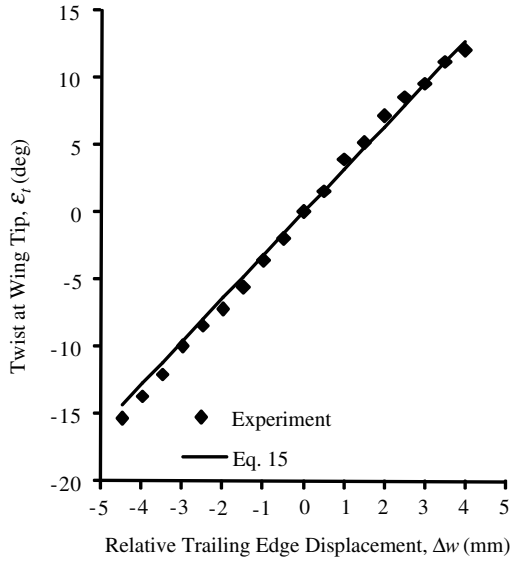

Fig. 8 Results for static deflection test.

B. Wind-Tunnel Tests

To determine the lift and drag characteristics of the warping wing, a wind-tunnel experiment was carried out at the Delft University of Technology low-speed, low-turbulence wind tunnel, an atmospheric tunnel of the closed-throat single-return type, with a contraction ratio of 17.8. The overall objective of this test was to demonstrate that the warping mechanism would indeed alter the aerodynamic properties of the wing. The octagonal test section measured 1.80 m in width, 1.25 m in height, and 2.60 m in length. The wing was clamped vertically against a mechanically actuated turntable flush with the test-section top wall. Measurements were taken by a six-axis balance. The test setup is displayed in Fig. 9.

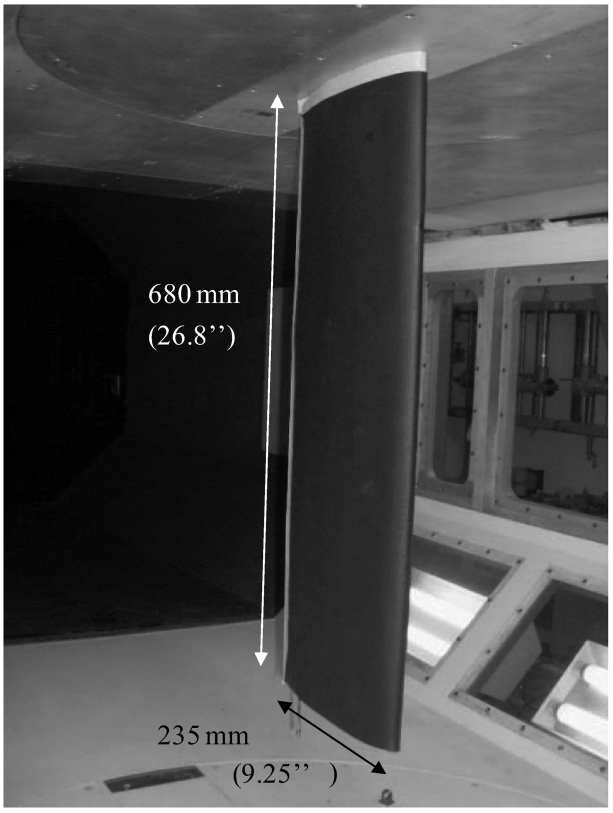

a) Isometric view

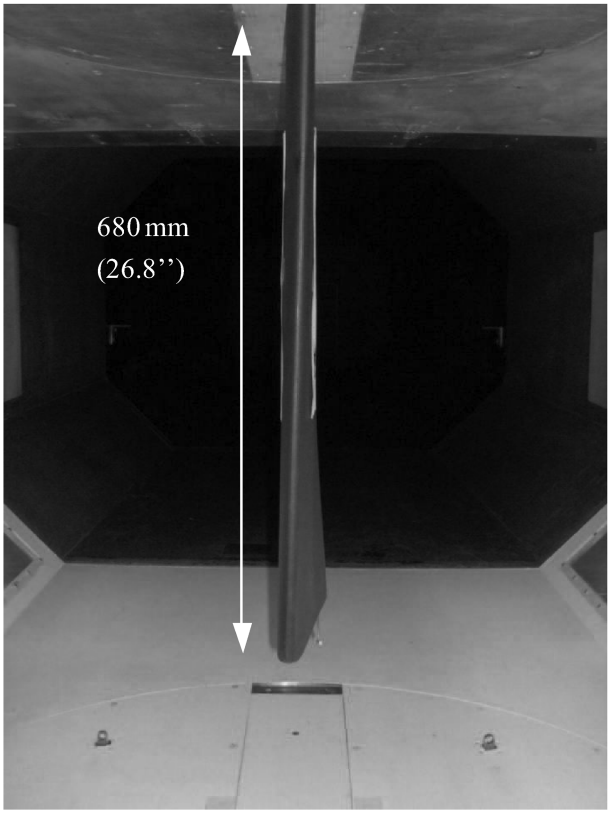

b) Front view of twisted wing

Fig. 9 Wind-tunnel experimental setup.

Measurements were taken at a velocity of 15 m/s (Reynolds number of 2.6×10^5) for angles of attack ranging from -2 to $+20°$. From the obtained data, the relation between the trailing-edge warping displacement Δw and lift coefficient C_L is plotted for four angles of attack (see Fig. 10), along with the analytic and vortex-lattice predictions. The results show that both the analytic and the vortex-lattice predictions display a linear behavior of the lift coefficient with the relative trailing-edge displacement Δw. For small absolute Δw, the correspondence between theory and experiment was accurate. At higher absolute values of Δw, a deviation from this linear trend was observed. This deviation was attributed to the change in wing-section shape induced by the warping of the wing [24]. That is, both models assumed a constant airfoil section over the span of the wing. In reality, however, there was an observable change in the airfoil shape at either end of the wing from the original NACA 23012 shape, as might also be observed from Figs. 7a and 7b.

Drag measurements compared with the analytic predictions are shown in Fig. 11. As long as attached flow was present, the analytic approximation as given by Eqs. (13) and (14) showed good correlation with the experimental results. It can be observed that separation occurred at zero angle of attack and negative twist angles (negative warping displacements), resulting in a higher drag coefficient than anticipated by the analytic model. This graph shows that a significant change in drag coefficient can be achieved by changing the twist of the wing by means of warping. Aerodynamic wing efficiency represented in terms of the lift-to-drag ratio as a function of the relative trailing-edge displacement is shown in Fig. 12. The figure shows that L/D increases with twist angle at lower angles of attack. A more positive twist angle (or washin) therefore results in higher wing efficiency. This corresponds well with the analytic prediction that was found from the ratio between Eqs. (11) and (13).

In general, the wind-tunnel results demonstrated that the warping wing mechanism could provide a substantial amount of lift change. The maximum change in lift that could be achieved by means of wing warping was constant with angle of attack at approximately $\Delta C_L = 0.7$. For small amounts of warping, -2 mm $< \Delta w < 2$ mm and $C_{L_{\epsilon_t}} = 0.032$ 1/ deg, which was constant with angle of attack. Furthermore, wind-tunnel tests proved that wing warping can play

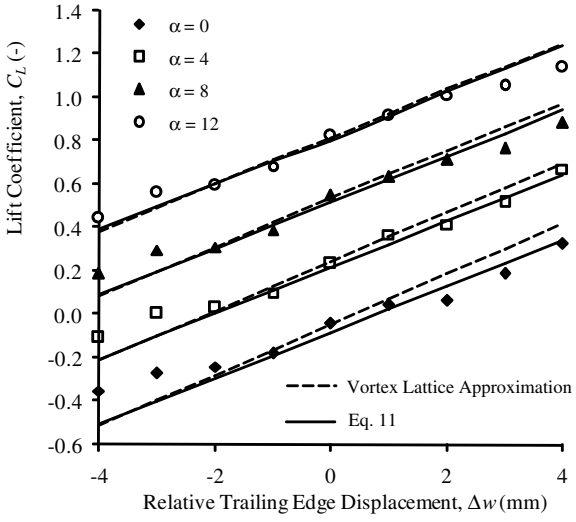

Fig. 10 Results for lift coefficient.

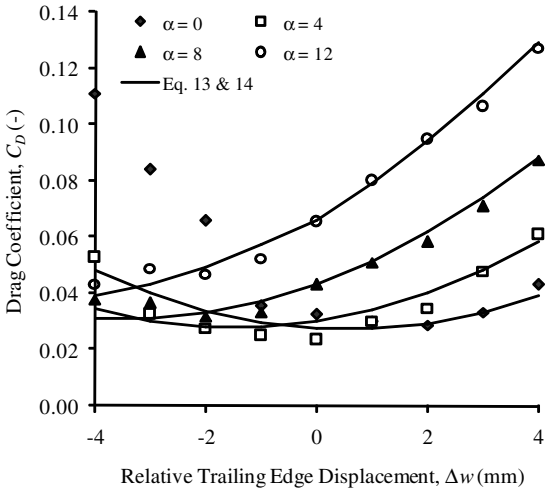

Fig. 11 Results for drag coefficient.

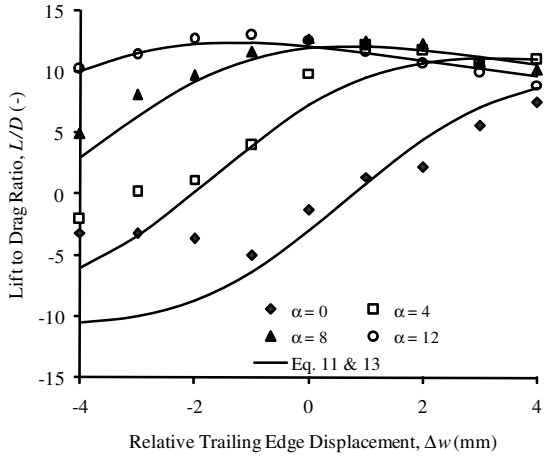

Fig. 12 Results for lift-to-drag ratio.

an active roll in decreasing the lift-induced drag on the wing or increasing the lift-to-drag ratio.

VI. Conclusions

A new concept for actively controlling wing twist based on introducing warping displacement has been discussed. It was demonstrated analytically that the amount of energy required to induce a certain amount of twist in a wing can be significantly reduced if warping of the skin is not constrained by creating an open section. This feature could be integrated in a typical straight wing by creating a slit at the trailing edge that separated the upper and lower skins. A thread-rod mechanism was positioned near the slit to connect the lower and upper skins so that torsional stiffness of the wing was maintained while allowing the relative displacement between the upper and lower skins. This resulted in a linear relation between wing twist and relative trailing-edge warping displacement, which closely correlated to analytic predictions. The maximum peak-to-peak twist angle was measured to be 27 deg. Wind-tunnel tests on a 0.68-m-span demonstration wing showed that wing twist could change the lift coefficient by as much as 0.7 for angles of attack ranging from 0–12 deg. Analytical and vortex-lattice models were demonstrated to give accurate predictions of the lift coefficient at smaller absolute twist angles. More accurate predictions were obtained if the change in airfoil section due to warping was included in the models. Furthermore, analytic modeling of the wing drag was shown to be in close correspondence to the drag measurements and showed that wing warping could be used to change the lift-induced drag. In general, it was demonstrated that a more positive twist resulted in a higher lift-to-drag ratio, especially at lower angles of attack. This study demonstrated that a twist-active wing can have sufficient gain to control the rolling motion of an aircraft and to ensure that the lift-to-drag ratio is maximized at various flight conditions, while keeping energy requirements on the flight control actuators at a minimum.

Acknowledgments

This study was sponsored by the Faculty of Aerospace Engineering at Delft University of Technology. The authors would like to thank Leo Veldhuis and Leo Molenwijk for their assistance with the wind-tunnel experiments. Furthermore, the authors would like to acknowledge the contribution of the technical staff of the Faculty of Aerospace Engineering.

References

[1] Phillips, W. F., Alley, N. R., and Goodrich, W. D., "Lifting-Line Analysis of Roll Control and Variable Twist," *Journal of Aircraft*, Vol. 41, No. 5, 2004, pp. 1169–1176. doi:10.2514/1.3846

[2] Garcia, H., Abdulrahim, M., and Lind, R., "Roll Control for a Micro Air Vehicle Using Active Wing Morphing," AIAA Guidance, Navigation, and Control Conf. and Exhibit, AIAA Paper 2003-5347, Austin, TX, 11–14 Aug. 2003.

[3] Phillips, W. F., "Lifting-Line Analysis for Twisted Wings and Washout-Optimized Wings," *Journal of Aircraft*, Vol. 41, No. 1, 2004, pp. 128–136. doi:10.2514/1.262

[4] Phillips, W. F., Fugal, S. R., and Spall, R. E., "Minimizing Induced Drag with Geometric and Aerodynamic Twist, CFD Validation," 43rd AIAA Aerospace Sciences Meeting and Exhibit, AIAA Paper 2005-1034, Reno, NV, Jan. 2005.

[5] Gould, D. K., "Mission Adaptive Wing Flight Demonstration Program," *SAE Aerospace Congress and Exposition*, SAE International Paper 811035, Anaheim CA, 1981.

[6] DeCamp, R. W., and Hardy, R., "Mission Adaptive Wing Advanced Research Concepts," *AIAA Atmospheric Flight Mechanics Conference*, AIAA, Washington, D.C., 1984, pp. 465–470.

[7] Perry, R., Cole, S., and Miller, G., "Summary of an Active Flexible Wing Program," *Journal of Aircraft*, Vol. 32, No. 1, Feb. 1995, pp. 10–15. doi:10.2514/3.46677

[8] Andersen, G., Forster, E., Kolonay, R., and Eastep, F., "Multiple Control Surface Utilization in Active Aeroelastic Wing Technology," *Journal of Aircraft*, Vol. 34, No. 4, 1997, pp. 552–557. doi:10.2514/2.2208

[9] Pendleton, E., Bessett, D., Field, P., Miller, G., and Griffin, K., "Active Aeroelastic Wing Flight Research Program: Technical Program and Model Analytical Development," *Journal of Aircraft*, Vol. 37, No. 4, 2000, pp. 554–561. doi:10.2514/2.2654

[10] Schweiger, J., and Suleman, A., "The European Research Project Active Aeroelastic Aircraft Structures," *CEAS/AIAA/NVvL International Forum on Aeroelasticity and Structural Dynamics*, Netherlands Association of Aeronautical Engineers, Amsterdam, 2003.

[11] Florance, J., Heeg, J., Spain, C., Ivanco, T., Wieseman, C., and Lively, P., "Variable Stiffness Spar Wind-Tunnel Model Development and Testing," 45th AIAA Structures, Structural Dynamics and Materials Conf., AIAA Paper 2004-1588, Palm Springs, CA, 19–22 April 2004.

[12] Chen, P., Sarjaddo, D., Jha, R., Lui, D., Griffin, K., and Yurkovich, R., "Variable Stiffness Spar Approach for Aircraft Maneuver Enhancement Using ASTROS," *Journal of Aircraft*, Vol. 37, No. 5, 2000, pp. 865–871. doi:10.2514/2.2682

[13] Vos, R., Hodigere-Siddaramaiah, V., and Cooper, J., "Aeroelastic Flight Control for Subscale UAVs," 48th AIAA/ASME/ASCE/AHS/ASC Structures, Structural Dynamics, and Materials Conf., AIAA Paper 2007-1706, Waikiki, HI, 23–27 April 2007.

[14] Vu, P., and Chavez, F., "Investigation of the Effects of Stiffness on Control Power via a Morphing Wing Technology," 46th AIAA/ASME/ASCE/AHS/ASC Structures, Structural Dynamics and Materials Conf., AIAA Paper 2005-2039, Austin, TX, 2005.

[15] Bisplinghoff, R., Ashley, H., and Halfman, R. L., "Introduction to Aeroelasticity," *Aeroelasticity*, Dover, New York, 1955.

[16] Giurgiutiu, V., and Rogers, G. A., "Large-Amplitude Rotary Induced Strain (LARIS) Actuator," *Journal of Intelligent Material Systems and Structures*, Vol. 8, Jan. 1997, pp. 41–50. doi:10.1177/1045389X9700800105

[17] Megson, T., "Torsion of Solid Sections," *Aircraft Structures for Engineering Students*, 3rd ed., Butterworth-Heinemann, Oxford, 2001.

[18] Bisplinghoff, R., Ashley, H., and Halfman, R. L., "Airplane Structures Under Static Loads," *Aeroelasticity*, Dover, New York, 1955.

[19] Megson, T., "Bending, Shear and Torsion of Open and Closed, Thin-Walled Beams," *Aircraft Structures for Engineering Students*, 3rd ed., Butterworth-Heinemann, Oxford, 2001.

[20] Roskam, J., "Lift and Pitching Moment Prediction Methods," *Airplane Design, Part VI: Preliminary Calculation Aerodynamic, Thrust and Power Characteristics*, DARCorporation, Lawrence, KS, 1990.

[21] Roskam, J., "Drag Polar Prediction Methods," *Airplane Design, Part VI: Preliminary Calculation Aerodynamic, Thrust and Power Characteristics*, DARCorporation, Lawrence, KS, 1990.

[22] Melin, T., *Tornado, a Vortex-Lattice MATLAB Implementation for Linear Aerodynamic Wing Applications*, M.S. Thesis, Royal Inst. of Technology (KTH), Stockholm, Dec. 2000.

[23] Roskam, J., "Wing Layout Design," *Airplane Design, Part III, Layout Design of Cockpit, Fuselage, Wing and Empennage: Cutaways and Inboard Profiles*, DARCorporation, Lawrence, KS, 2002.

[24] Loeven, G., and Bijl, H., "Airfoil Analysis with Uncertain Geometry Using the Probabilistic Collocation Method," 49th AIAA/ASME/ASCE/AHS/ASC Structures, Structural Dynamics, and Materials Conf., AIAA Paper 2008-2070, Schaumburg, IL, 7–10 April 2008.